ACS Catalysis

Research Article

Cite This: ACS Catal. 2019, 9, 1437−1445

pubs.acs.org/acscatalysis

Insights into the Activation Effect of H_2 Pretreatment on Ag/Al_2O_3 Catalyst for the Selective Oxidation of Ammonia

Fei Wang,[†,‡] Guangzhi He,[†] Bo Zhang,[†] Min Chen,[†] Xueyan Chen,[†,‡] Changbin Zhang,[*,†,§] and Hong He[†,‡,§]

[†]State Key Joint Laboratory of Environment Simulation and Pollution Control, Research Center for Eco-Environmental Sciences, Chinese Academy of Sciences, Beijing 100085, China

[‡]University of Chinese Academy of Sciences, Beijing 100049, China

[§]Center for Excellence in Regional Atmospheric Environment, Institute of Urban Environment, Chinese Academy of Sciences, Xiamen 361021, China

Supporting Information

ABSTRACT: The Ag/Al_2O_3 catalyst possesses high activity for selective catalytic oxidation of ammonia (NH_3−SCO), and its activity could be significantly improved by H_2 pretreatment. It is generally accepted that the enhancement of Ag/Al_2O_3 activity after H_2 reduction is due to the promoted O_2 activation by metallic Ag species. Here, we show that the recovery of Brønsted acid sites via H_2 reduction is also an important factor. Ag/Al_2O_3 and H_2-pretreated Ag/Al_2O_3 (Ag/Al_2O_3−H_2) catalysts were prepared and tested for the NH_3−SCO performances, and also carefully characterized. It is revealed that Ag species were anchored on the Al_2O_3 surface through exchange between Ag^+ and H^+ in AlOH groups during the preparation process, and therefore occupied the Brønsted acid sites of Al_2O_3. H_2 reduction could break the Ag−O bonds and thus recover the Brønsted acid sites. *In situ* DRIFTS results show that NH_4^+ species adsorbed on Brønsted acid sites is much more active for reaction with O_2 than NH_3 species adsorbed on Lewis acid sites. DFT calculation results identified the different activation processes for NH_4^+ and NH_3 species, confirming that Brønsted acid sites have markedly higher activity than the Lewis acid sites. Therefore, the recovery of Brønsted acid sites after H_2 reduction is also responsible for the improved activity of Ag/Al_2O_3−H_2 for NH_3−SCO.

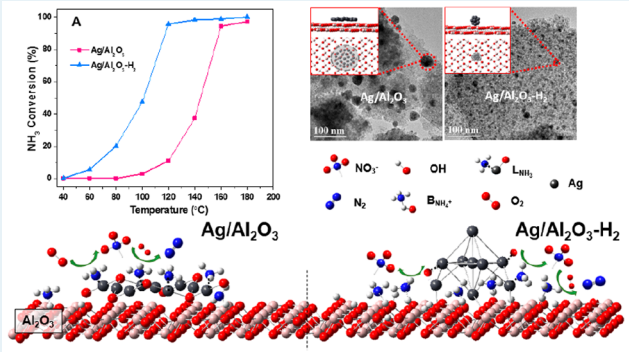

KEYWORDS: *ammonia (NH_3), Ag/Al_2O_3, H_2 pretreatment, Ag anchoring, acid site*

1. INTRODUCTION

NH_3 is widely used in the chemical industry (nitric acid production, petroleum refining), agriculture (nitrogen fertilizer), and the transportation industry (deNO_x process), where it is inevitably emitted due to the ammonia slip phenomenon. The pungent gas NH_3 is harmful to human health as well as the environment. It is one of the most important nitrogen-containing pollutants and is also a significant contributor of haze formation in China.[1−4] Therefore, it is essential to control the NH_3 emission.

Various methods have been proposed for NH_3 elimination,[5−8] among which NH_3−SCO is a very promising one, in consideration of the technical and economic limitations. Recently, the NH_3−SCO method has raised widespread concern, and many kinds of catalysts have been investigated. Ag/Al_2O_3 catalyst has shown high activity in several studies,[9−16] which was even better than several noble metal catalysts.[10,11] Our previous studies[14,17,18] showed that particle size and valence state of Ag species were two important factors for NH_3−SCO activity and N_2 selectivity. H_2 pretreatment is the most common method to change Ag from the oxidized state to the metallic state, and significant enhancement of NH_3−SCO activity can be observed after H_2 pretreatment.[11,14] The enhancement was simply attributed to the appearance of metallic Ag, promoting O_2 activation. However, the effect of other aspects such as Ag particle size, active sites and acid sites on the performance of Ag based catalyst has received little attention to date. The influence of H_2 pretreatment on the NH_3−SCO pathway has also not been clearly investigated in the previous studies.

In order to fill in the knowledge gaps mentioned above, fresh Ag/Al_2O_3 and H_2-pretreated Ag/Al_2O_3 were prepared and tested, and then characterized by several methods such as X-ray diffraction (XRD), high-resolution transmission electron microscope (HR-TEM), X-ray absorption fine structure spectroscopy (XAFS) and *in situ* diffuse reflectance infrared

Received: September 17, 2018
Revised: December 17, 2018
Published: January 7, 2019

DOI: 10.1021/acscatal.8b03744
ACS Catal. 2019, 9, 1437−1445

Fourier transform spectroscopy (DRIFTS). The detailed effects of H_2 pretreatment on Ag particle size, active sites and acid sites were studied. On the basis of these findings, the reaction pathway of NH_3−SCO on Ag/Al_2O_3 and Ag/Al_2O_3−H_2 were also investigated.

2. EXPERIMENTAL SECTION

2.1. Catalyst Preparation. According to our previous studies,[14,17] we selected and prepared 10 wt % Ag/Al_2O_3 to study the effect of H_2 reduction on NH_3−SCO performance, and the Ag/Al_2O_3 (2, 4, and 8 wt %) were also prepared for investigating the properties of acid sites and Ag species anchoring. Ag was deposited onto a γ-Al_2O_3 (Sigma-Aldrich, average size 5 μm) support by an impregnation method. First, appropriate amounts of γ-Al_2O_3 were added into deionized water to stir into suspension, then aqueous solutions of $AgNO_3$ with different loading contents were introduced. After impregnation for 3 h, the suspension was dried with vacuum rotary evaporation. After drying for 12 h at 105 °C and calcination in air for 3 h at 500 °C, the samples were finally sieved into 40−60 mesh powders.

Fresh Ag/Al_2O_3 were treated with H_2/N_2 (20 vol % H_2, 100 $cm^3 \cdot min^{-1}$) at 400 °C for 2 h and the H_2-reduced samples was denoted as Ag/Al_2O_3−H_2.

2.2. Sample Characterization. The crystal structures of the catalysts were measured on a Bruker D8 X-ray diffractometer with a Cu Kα radiation source (λ = 0.15406 nm) (2θ: 10−90°, scanning speed: 6°·min^{-1}). HR-TEM images were collected on a JEOL JEM-2010 instrument (acceleration voltage: 200 kV).

Ag K-edge XAFS measurements were conducted at the BL14W1 XAFS beamline of Shanghai Synchrotron Radiation Facility (SSRF) (PE storage ring was operated at 3.5 GeV with 200 mA). Athena program[19,20] was used to analyze the XAFS data, and the filtered k^2 weighted $\chi(k)$ was Fourier transformed into R space (k range: 2.2−12.8 $Å^{-1}$ for Ag−K EXAFS).

NEXUS 670-FTIR equipped with an MCT/A detector was used to perform the *in situ* DRIFTS to research the NH_3−SCO reaction mechanism. Before the measurement, the sample was pretreated with 20 vol % O_2/N_2 at 500 °C for 30 min or prereduced with 20 vol % H_2/N_2 at 400 °C for 2 h.

2.3. Catalytic Test. A fixed-bed reactor was used to test the NH_3−SCO activity of the catalysts, the total gas flow was 100 mL·min^{-1} and gas hourly space velocity (GHSV) was 28 000 h^{-1}. The mixture gas is composed of 500 ppm of NH_3, 10 vol % O_2 and N_2 as balance. The concentrations of effluent NH_3 and NOx were continuously monitored with an online FTIR spectrometer. Only NO, NO_2, N_2O, and NH_3 were detected during the reaction process; therefore, NH_3 conversion (X_{NH_3}) and N_2 selectivity (S_{N_2}) were calculated according to the following formulas:

$$X_{NH_3} = 1 - \frac{[NH_3]_{out}}{[NH_3]_{in}} \times 100\% \quad (1)$$

$$S_{N_2} = \frac{[NH_3]_{in} - 2[N_2O]_{out} - [NO_2]_{out}[NO]_{out}}{[NH_3]_{in}} \times 100\% \quad (2)$$

2.4. DFT Computational Details. Spin-polarized density functional theory (DFT) calculations were conducted through the PBE functional[21] with van der Waals correction (i.e., DFT-D3 method with Becke−Jonson damping)[22] as implemented in the VASP 5.4.1.[23] The core−valence electron interaction was described with projector augmented wave (PAW) method[24] and the energy cutoff of the plane wave basis sets was set to 400 eV for all atoms. A supercell of the γ-Al_2O_3 (110) surface with four stoichiometric Al_2O_3 layers (about 16 × 11 × 6 Å) was used as the substrate. We modeled the Ag cluster (5 Ag atoms) supported on γ-Al_2O_3 surfaces and it was added to one side of the slab. In order to avoid the periodic image interaction normal to the surface, a vacuum gap of 12 Å was applied.[25] Structures were optimized with a conjugate gradient algorithm until the forces on all relaxed atoms were less than 0.02 eV/Å. During the structural optimization, the bottom Al_2O_3 layer was kept frozen while other atoms were fully relaxed, only the Γ point of the Brillouin zone was sampled. In order to accelerate electronic convergence, the Gaussian smearing method was applied with a smearing width of 0.2 eV. The CI-NEB method was used to trace the reaction pathways and locate the transition states, the spring constant was 5.0 eV/$Å^2$.[26,27]

3. RESULTS

3.1. Results of Catalytic Tests. The NH_3−SCO activity of Ag/Al_2O_3 and Ag/Al_2O_3−H_2 were evaluated and presented in Figure 1. It was clear that the activity was significantly improved after H_2 pretreatment and the T_{50} (the temperature of 50% NH_3 conversion) of NH_3−SCO decreased from 145 to 100 °C. The selectivity of N_2 declined to some extent after H_2 reduction, but it was still above 80%. The decrease of N_2 selectivity was due to the generation of more N_2O resulted

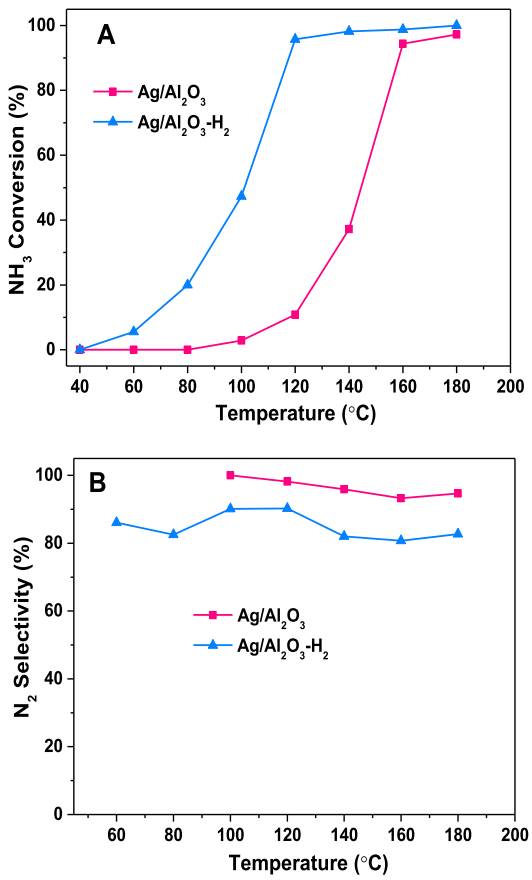

Figure 1. (A) NH_3 conversion (B) N_2 selectivity at different temperatures over 10% Ag/Al_2O_3 and Ag/Al_2O_3−H_2 samples.

DOI: 10.1021/acscatal.8b03744
ACS Catal. 2019, 9, 1437−1445

from the overoxidation of NH_3 by more oxygen species activated on metallic Ag species. These results show that H_2 reduction can greatly enhance the NH_3−SCO performance of Ag/Al_2O_3 catalyst, which have been generally attributed to the promoted O_2 activation by appearance of metallic Ag species.[11,14,28]

3.2. Results of Characterization. *3.2.1. Structural Properties.* XRD patterns of the Al_2O_3, Ag/Al_2O_3, and Ag/Al_2O_3−H_2 samples are presented in Figure 2. The diffraction peaks at (220), (311), (222), (400), (511), (440), and (444) planes of γ-Al_2O_3 (JCPDS 02-1420) were observed on Al_2O_3 support. As for the Ag/Al_2O_3 sample, the intensity of the γ-Al_2O_3 peaks were weakened after Ag was loaded, and diffraction peaks of Ag species at 38.1°, 44.3°, 64.5° and 77.4° were observed with low intensity, which corresponded to the (111), (200), (220), and (311) lattice planes of crystalline Ag (JCPDS 87−0717). Ag_2O peaks did not appear in the XRD patterns mainly due to its low degree of crystallinity or the small particle size of Ag_2O below XRD detection limit. After H_2 reduction, the intensity of the Ag diffraction peaks increased dramatically and showed narrow half-widths, indicating that the ratio of the metallic Ag species was greatly improved.

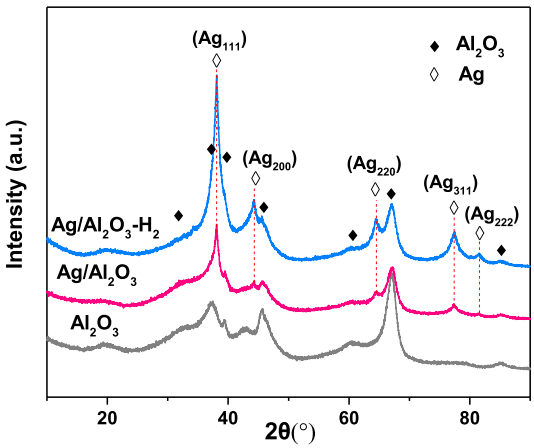

Figure 2. XRD profiles of Al_2O_3 support, 10% Ag/Al_2O_3 and Ag/Al_2O_3−H_2 samples.

Parts A and C of Figure 3 presented the TEM images of the Ag/Al_2O_3 and Ag/Al_2O_3−H_2. The morphology of Ag species was dramatically changed after H_2 pretreatment. In Ag/Al_2O_3, flaky Ag species covered the surface of Al_2O_3 with average particle size of 8.4 nm. In the corresponding HRTEM image (Figure 3 B), lattice fringes for Ag species were clearly visible with the lattice spacings of about 0.264 or 0.232 nm, which were consistent with the (100) and (011) planes of Ag_2O (JCPDS File No. 01-072-2108).[29] As shown in Figure 3C, Ag species was observed as highly dispersed on Ag/Al_2O_3−H_2 with a particle size of 5.4 nm. It was observed in the corresponding HRTEM image (Figure 3 D) that the lattice spacings were 0.236 and 0.203 nm, which were attributed to

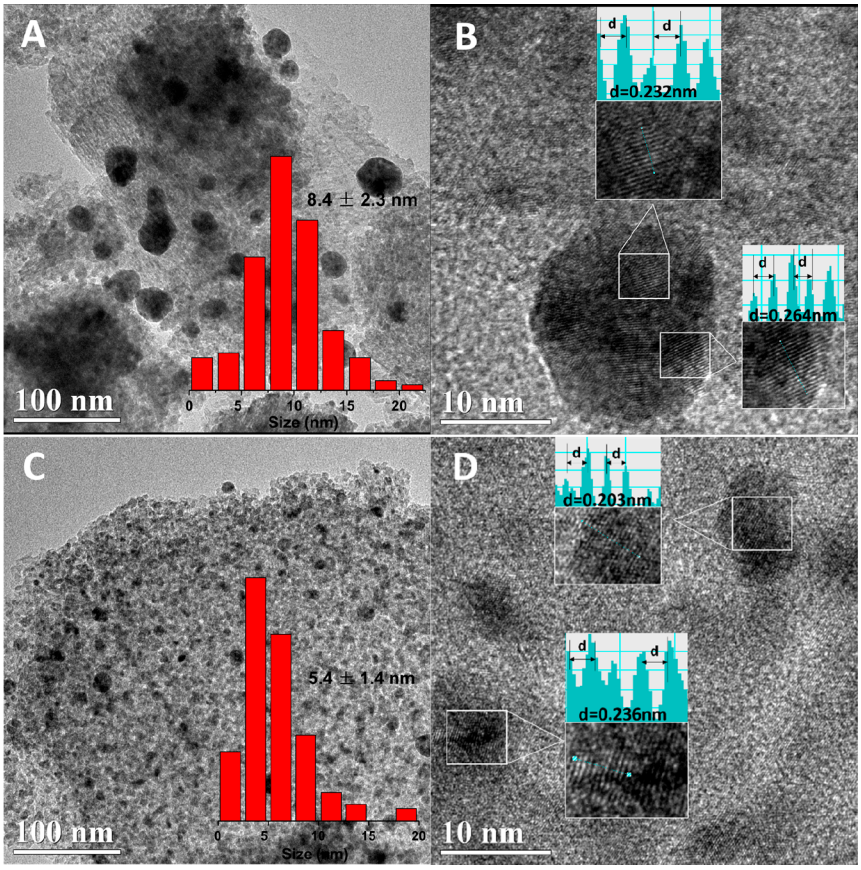

Figure 3. (A) Typical TEM images of 10% Ag/Al_2O_3 (inset shows the size distribution histograms), (B) corresponding HRTEM images of 10% Ag/Al_2O_3, (C) typical TEM images of 10% Ag/Al_2O_3−H_2 sample (inset shows the size distribution histograms), and (D) corresponding HRTEM images of 10% Ag/Al_2O_3−H_2.

DOI: 10.1021/acscatal.8b03744
ACS Catal. 2019, 9, 1437−1445

(111) and (200) planes of cubic metallic Ag (JCPDS File No. 01-071-3762),[29−31] respectively.

3.2.2. Chemical States. Figure 4 displays the Ag−K edge XAFS data of Ag/Al_2O_3 and $Ag/Al_2O_3-H_2$ together with Ag foil and $AgNO_3$ as references. The XANES result of Ag/Al_2O_3 in Figure 4A shows that the peaks and edge positions differ from both Ag foil and $AgNO_3$. The white line of Ag/Al_2O_3 was located at between those of Ag foil and $AgNO_3$, which indicated that Ag species in Ag/Al_2O_3 was a mixture of Ag^0 and Ag^+.[32] However, the spectrum of $Ag/Al_2O_3-H_2$ was much like that of Ag foil, and the intensity of the white line decreased and the position moved closer to Ag-foil after H_2 reduction. As shown in Figure 4B, the normalized first-order derivative peaks of Ag/Al_2O_3 and $Ag/Al_2O_3-H_2$ located at 25516.4 and 25515.7 eV, respectively, while the locations of Ag foil and $AgNO_3$ were 25514.9 and 25518.6 eV, respectively. Therefore, it was further confirmed that Ag existed as a mixture of Ag^0 and Ag^+ in Ag/Al_2O_3 sample, whereas after H_2 reduction Ag species in $Ag/Al_2O_3-H_2$ was nearly metallic state,[32,33] which was consistent with XRD and TEM results.

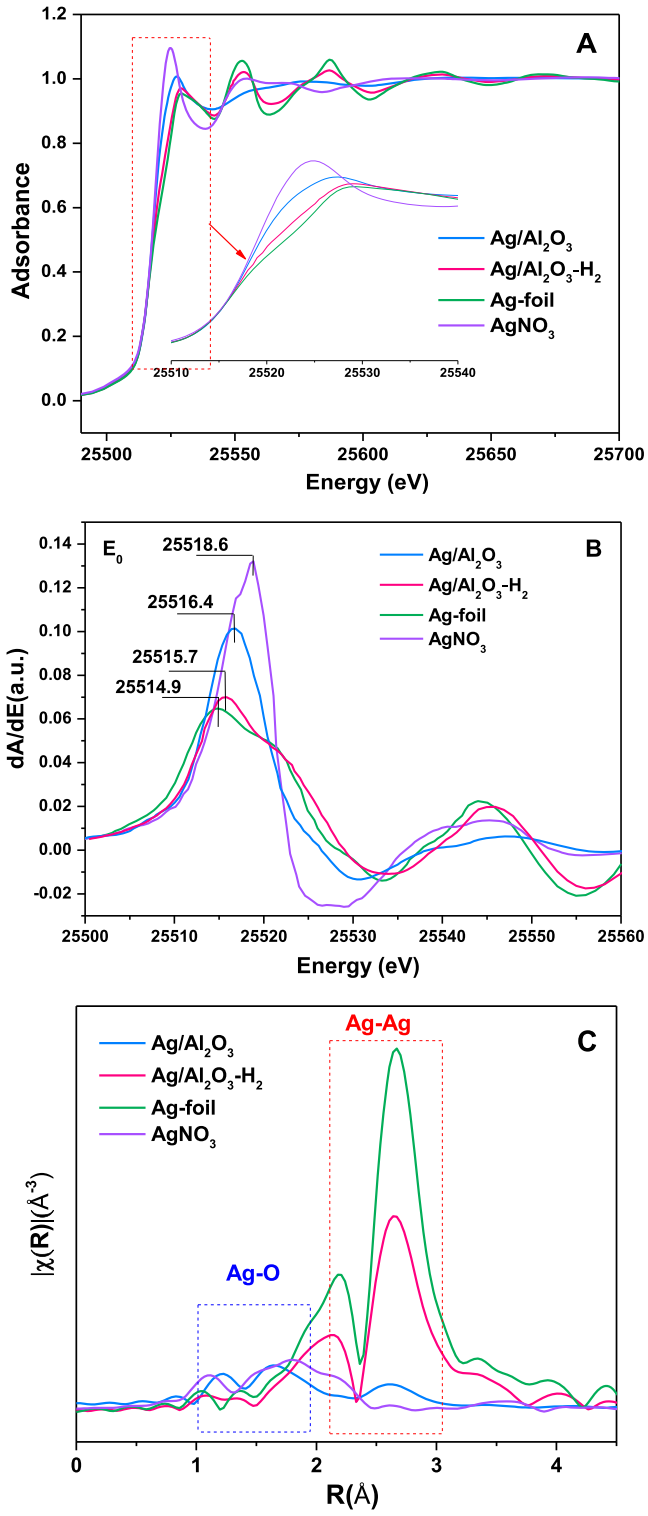

Figure 4. Ag−K edge XAFS spectra, (A) Normalized near-edge structure (XANES), (B) first-order derivatives, and (C) k^2 weighted EXAFS spectra of standard samples and 10% Ag/Al_2O_3, $Ag/Al_2O_3-H_2$ samples (Fourier transform k range 2.2−12.8 $Å^{-1}$).

Fourier transforms of k^2-weighted EXAFS spectra of Ag/Al_2O_3, $Ag/Al_2O_3-H_2$ and standard samples were shown in Figure 4 (C). The peaks at around 1.7 and 2.67 Å were attributed to Ag−O and metallic Ag−Ag bonding.[34,35] The intensity of the Ag−Ag shell was very low and the Ag−O shell was dominant in Ag/Al_2O_3 sample. However, the situation was just the reverse on the $Ag/Al_2O_3-H_2$ sample: the Ag−O shell was barely observed while the Ag−Ag shell was dominant, which was similar to the results for Ag foil. Therefore, we concluded that H_2 reduction breaks Ag−O bonds on the Ag/Al_2O_3 surface and forms Ag clusters in the metallic state (Ag_n^0).

3.2.3. Acid Sites. In situ DRIFTS of NH_3 adsorption were measured over Ag/Al_2O_3 and $Ag/Al_2O_3-H_2$ samples with different Ag content to distinguish the different acid types (Lewis or Brønsted acid sites) as presented in Figure 5. The bands located at 3100−3500 cm^{-1} were attributed to the N−H stretching vibration bands of NH_3.[13,36−38] The negative peaks at 3755 and 3678 cm^{-1} were resulted from the consumption of surface hydroxyl.[39] The bands of δ_{as} at 1616 cm^{-1} and δ_s at 1215 and 1252 cm^{-1} for the N−H bonds were assigned to coordinately linked NH_3 on Lewis acid sites (denoted as NH_3−L),[13,36,37,40] and the peaks at 1687, 1471, and 1394 cm^{-1} were assigned to vibrations of ionic NH_4^+ species bound to Brønsted acid sites (denoted as NH_4^+−B).[36,41,42] As shown in Ag/Al_2O_3 spectra, the intensity of the peaks related to NH_3−L

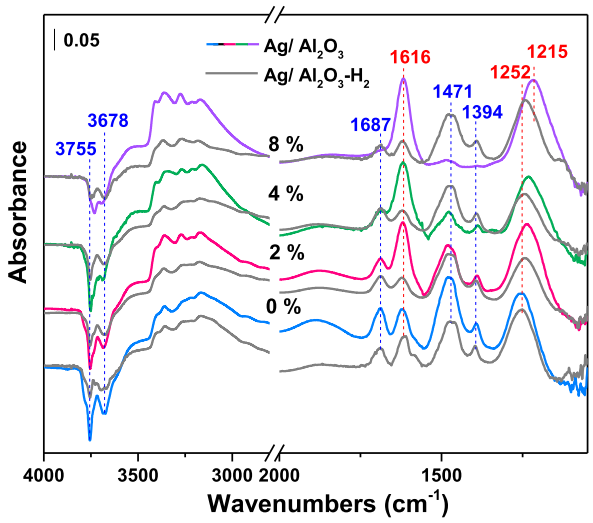

Figure 5. *In situ* DRIFTS results of NH_3 adsorption over Ag/Al_2O_3 and $Ag/Al_2O_3-H_2$ with different silver loadings at room temperature.

DOI: 10.1021/acscatal.8b03744
ACS Catal. 2019, 9, 1437−1445

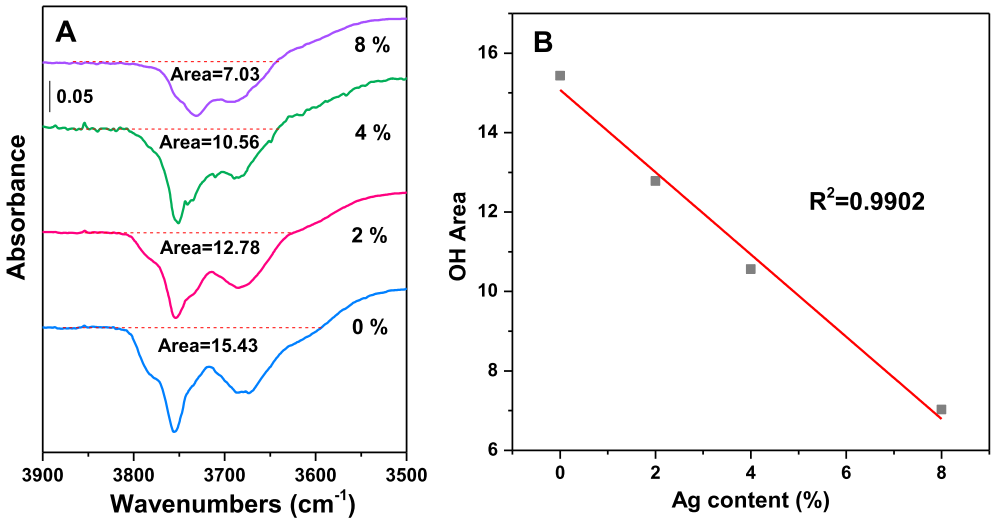

Figure 6. *In situ* DRIFTS analysis of hydroxyl content on $Ag/Al_2O_3-H_2$ samples with different Ag loadings with NH_3 as the probe molecule (A) and the linear fitting result of Ag content and hydroxyl peak area (B).

(1616, 1252, and 1215 cm^{-1}) increased gradually as the Ag load increased. On the contrary, the intensity of NH_4^+-B (1687, 1471, and 1394 cm^{-1}) decreased rapidly with Ag content increasing, and a corresponding decline was also observed in the intensity of OH consumption peaks (3755 and 3678 cm^{-1}). In addition, it was notable that the δ_s peak of NH_3-L shifted from 1252 to 1215 cm^{-1} as Ag was loaded onto Al_2O_3, which indicated that two kinds of Lewis acid sites (Al−O and Ag−O) existed on the Ag/Al_2O_3 sample.

As shown in the spectra of $Ag/Al_2O_3-H_2$ samples, a significant influence of H_2 reduction on acid sites can be observed. One of the most obvious changes was the growth of NH_4^+-B (1687, 1471, and 1394 cm^{-1}). Another effect of H_2 reduction on acid sites was equally striking: δ_{as} of NH_3-L decreased rapidly after H_2 reduction, along with the phenomenon that δ_s of NH_3-L shifted back from 1215 to 1252 cm^{-1}. Thus, it is suggested that Ag was anchored on the Al_2O_3 support through occupying Brønsted acid sites of Al_2O_3 and form Ag−O bonds, while the H_2 reduction could break those bonds and thus recover the Brønsted acid sites. However, the hydroxyl peaks intensities of $Ag/Al_2O_3-H_2$ samples could not totally recover to their original levels in fresh Ag/Al_2O_3. The loss of some surface hydroxyl should be induced by the high temperature H_2 reduction (400 °C) but not by Ag loading since the H_2 reduction also decreased the hydroxyl content of pure Al_2O_3.

3.2.4. Silver Anchoring. Ja Hun Kwak and co-workers have proposed that Pt atoms could bind to the Al^{3+}_{penta} sites on the γ-Al_2O_3 surface through oxygen bridges.[43] We measured the ^{27}Al solid state MAS NMR of γ-Al_2O_3 support and 10% Ag/Al_2O_3 sample. As shown in Figure S1 (Supporting Information), the intensity of Al^{3+}_{penta} was barely changed after Ag loading, indicating that Al^{3+}_{penta} centers was not the anchoring sites for Ag.

It is well established that $A1_2O_3$ surfaces contain various A1-OH groups,[44] and these surface hydroxyl groups contribute to metal dispersion and anchoring.[43,45] Figure 6 A showed the selected *in situ* DRIFTS of NH_3 adsorption in the range of 3500−3900 cm^{-1} over Ag/Al_2O_3 with different Ag contents at room temperature. The peak areas of hydroxyl groups (3755 and 3678 cm^{-1}) were calculated by integration and presented in Figure 6 A. It is obvious that the peak intensity of the Al−OH declined rapidly with the increase of Ag loadings. The correlation fitting between Ag loadings and hydroxyl peak area was next carried out. As shown in Figure 6 B, hydroxyl peak area presented a linear decrease as a function of Ag loadings, further indicating that Ag was anchored on the Al_2O_3 surface through the consumption of Al−OH groups.

3.3. Reaction Mechanism. Our previous study showed that Ag^0 in Ag/Al_2O_3 generated from H_2 pretreatment could promote O_2 dissociation,[13] which enhanced NH_3−SCO activity of $Ag/Al_2O_3-H_2$. We here observed that the change of acid sites resulted from H_2 pretreatment may be another reason for the enhanced NH_3−SCO activity. To investigate the specific reaction behaviors of the acid and active sites, the reaction between preadsorbed NH_3 and O_2 on Ag/Al_2O_3 and $Ag/Al_2O_3-H_2$ was studied by *in situ* DRIFTS.

The NH_3−SCO reaction pathway on fresh Ag/Al_2O_3 has already been studied and was described in our recent article.[17] It is indicated that after O_2 was introduced, nitrate bands appeared and monodentate nitrate could react with reintroduced NH_3, which was consistent with the i-SCR mechanism. The reaction pathway over $Ag/Al_2O_3-H_2$ was then studied. NH_3 was preadsorbed for 30 min at 120 °C and followed with N_2 purging for 30 min. As presented in Figure 7 A, the peaks of both NH_3-L (1616 and 1252 cm^{-1})[13,36,37,40] and NH_4^+-B (1687, 1471, and 1394 cm^{-1})[36,41,42,46] appeared on $Ag/Al_2O_3-H_2$. No significant decrease was observed after N_2 purging for 15 min, which indicated that both of them were stably adsorbed. After that, O_2 was introduced into the system as presented in Figure 7 B, the peak of NH_4^+ ad-species decreased rapidly and disappeared within 10 min, while the peak intensity of coordinated NH_3 barely changed in the first 10 min, which indicated that the activity of NH_4^+ was far higher than coordinated NH_3. The consumption rates of Brønsted and Lewis acid sites peaks area were fitted in Figure 7 C. As can be seen, the decline slops of Lewis and Brønsted acid sites area were 0.203 and 1.009, respectively. It is to say that the consumption rate of NH_4^+ ad-species was almost 5 times as fast as that for coordinated NH_3. After O_2 was introduced for 30 min, both NH_3 species were exhausted, and broad peaks at 1443 and 1306 cm^{-1} were observed, which were very near to those of monodentate nitrate (1450 and 1286 cm^{-1}).[47−50]

DOI: 10.1021/acscatal.8b03744
ACS Catal. 2019, 9, 1437−1445

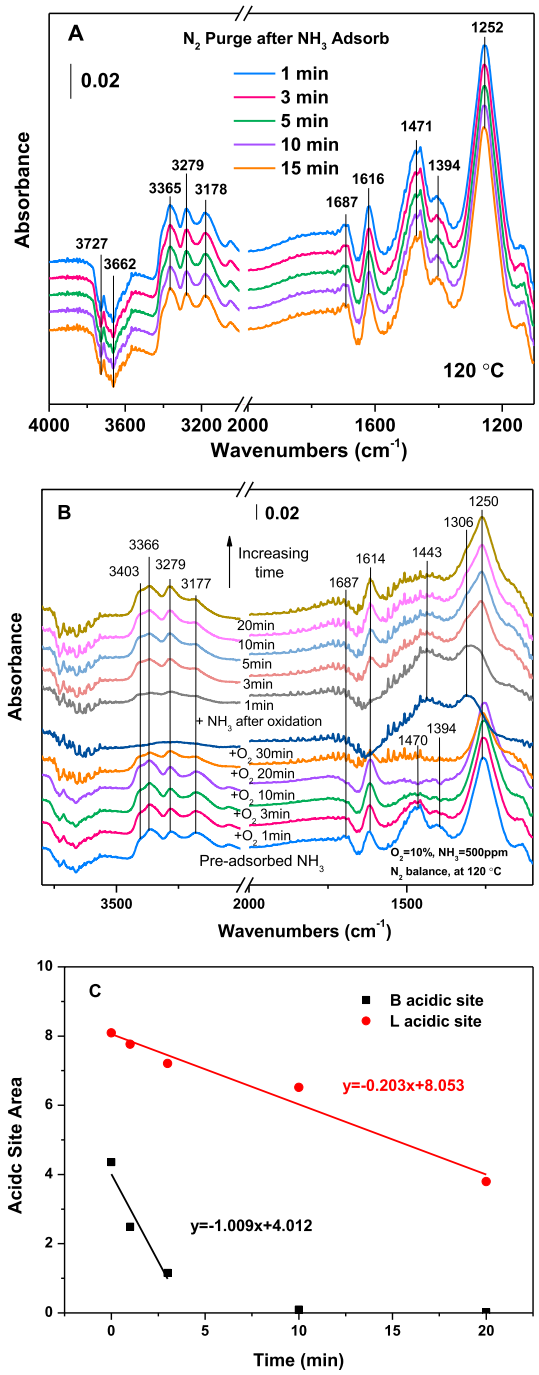

Figure 7. *In situ* DRIFTS results of (A) N_2 purge after NH_3 adsorption over 10% $Ag/Al_2O_3-H_2$ at 120 °C, (B) reaction between O_2 and preadsorbed NH_3 species and further reaction between NH_3 and in situ formed nitrate over 10% $Ag/Al_2O_3-H_2$ at 120 °C. Reaction conditions: $[NH_3]$ = 500 ppm, O_2 = 10%, and N_2 balance. (C) Consumption rate of peaks area of B and L acid sites.

When NH_3 was reintroduced, the nitrate peaks quickly declined, consistent with the phenomenon observed on fresh Ag/Al_2O_3. Thus, the NH_3−SCO mechanism over $Ag/Al_2O_3-H_2$ was also the i-SCR mechanism at 120 °C.

Previous studies have shown that the NH_3−SCO follows the −NH and i-SCR mechanism at low and high temperatures, respectively.[13] Therefore, in situ DRIFTS experiments at different temperatures were further conducted to research the effect of temperature on reaction mechanism. NH_3 adsorption on Ag/Al_2O_3 and $Ag/Al_2O_3-H_2$ samples were first measured at different temperatures. As shown in Figure S2 (Supporting Information), the peak positions of NH_3−L and NH_4^+−B were not changed with increasing temperatures, showing that those kinds of acid sites were unchanged at different temperatures. The decreases of the peak intensities were ascribed to desorption of the NH_3 species at higher temperature.

The *in situ* DRIFTS experiments of NH_3−SCO were next performed at three different temperatures (50, 100, and 160 °C) over $Ag/Al_2O_3-H_2$. NH_3 was preadsorbed at 50, 100, and 160 °C for 30 min and followed with N_2 purging for 20 min. After that, O_2 was introduced into the system. As shown in Figure S3 (Supporting Information), only NH_4^+ species (1470 cm^{-1}) were consumed but without the formation of any nitrate species at 50 °C, indicating that the pathway of NH_3−SCO on $Ag/Al_2O_3-H_2$ might also have followed the −NH mechanism at low temperature, and the NH_4^+ species could be dissociated into −NH with the assistance of oxygen and then formed the final N_2 or N_2O at low temperatures. NH_4^+−B was also more reactive than NH_3−L at 50 °C since no reaction occurred on Lewis acid sites. When the temperature was increased to 100 and 160 °C, the nitrate was obviously formed, and the nitrate could next react with NH_3 to yield final products, which is consistent with the i-SCR mechanism.

Although the NH_3−SCO pathways on Ag/Al_2O_3 and $Ag/Al_2O_3-H_2$ both followed the i-SCR mechanism at high temperatures, there may exist some differences in NH_3−SCO reaction pathways on Brønsted and Lewis acid sites since the activities of NH_3−L and NH_4^+−B were much different from each other. We then carried out the kinetic testing and calculated the apparent activation energy (E_a) of the reactions on the Ag/Al_2O_3 and $Ag/Al_2O_3-H_2$ catalysts. As presented in Figure S5 (Supporting Information), the E_a on $Ag/Al_2O_3-H_2$ (56.5 kJ/mol) was lower than that on Ag/Al_2O_3 sample (74.8 kJ/mol), confirming the different reaction pathways between two samples.

3.4. DFT Calculation. As for the i-SCR mechanism, adsorbed NH_3 would be activated by the active oxygen to form NH_{ad} species and then it will be oxidized into nitrate. Finally, the generated nitrate will react with NH_{ad} to form N_2 and H_2O. Thus, the main difference of NH_3−SCO reaction pathways on Brønsted and Lewis acid sites may exist in the activation process for NH_4^+ and NH_3 species. The different reaction pathways of NH_3−L and NH_4^+−B were identified using density functional theory (DFT) calculations. On Lewis acid sites, an H atom transferred from the adsorbed NH_3 to the surface O on the Ag cluster and thus generated an NH_2 species at the Al sites (Figure 8). On Brønsted acid sites, the NH_4^+ species moved from the Al_2O_3 support to the Ag cluster, with one H atoms being transferred to the surface O on the Ag cluster (Figure 9A). Then another H atom of the adsorbed NH_3 further transferred to surface O, resulted in the formation of an NH_2 species on the Ag cluster (Figure 9B). The overall energy barrier for the dissociation of NH_4^+−B was 0.64 eV, much lower than that for NH_3−L dissociation (1.02 eV). Therefore, the results of DFT calculations showed that the activity of Brønsted acid sites was markedly higher than the Lewis acid sites, which was in accordance with our experimental results (Figure 7).

4. DISCUSSION

The Ag/Al_2O_3 catalyst was prepared by an impregnation method and a H_2-pretreated sample was comparatively studied.

DOI: 10.1021/acscatal.8b03744
ACS Catal. 2019, 9, 1437−1445

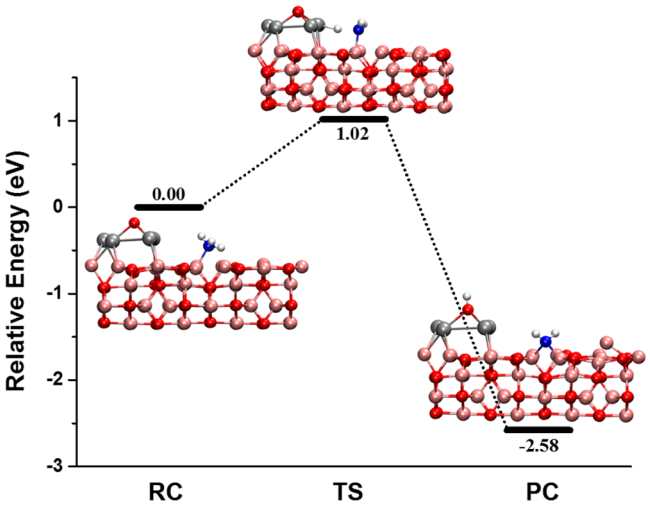

Figure 8. Energy profiles of the reaction pathway of NH_3 dissociation at Lewis acid sites as well as the optimized geometries of the reactant, transition state, and product. Silver, pink, red, blue, and white circles denote Ag, Al, O, N, and H atoms, respectively.

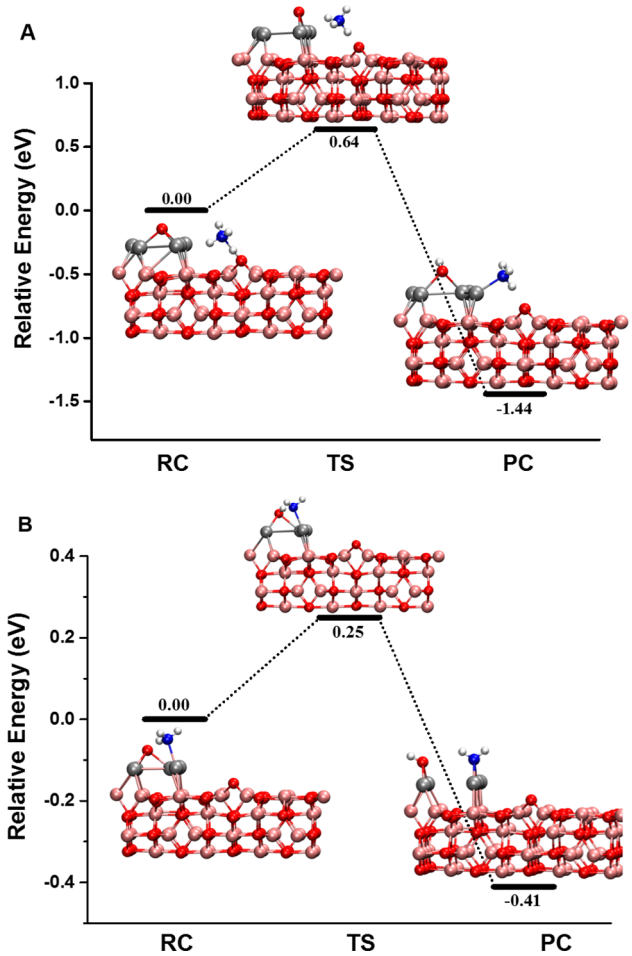

Figure 9. Energy profiles of the reaction pathway of NH_3 dissociation at Brønsted (surface Al−OH sites) acid sites as well as the optimized geometries of the reactant, transition state, and product. Silver, pink, red, blue, and white circles denote Ag, Al, O, N, and H atoms, respectively.

The characterization results of XRD, TEM, and XFAS showed that Ag species changed from oxidized state into metallic state after H_2 pretreatment, and the average Ag particle size was decreased dramatically. The XAFS results revealed that the dominant Ag−O coordination in Ag/Al_2O_3 disappeared in the $Ag/Al_2O_3-H_2$ sample, accompanied by an increase of Ag−Ag coordination. In addition, the results of acid sites tests revealed that Ag loading resulted in the decrease of OH groups and NH_4^+−B. Besides of that, the IR absorption peaks of NH_3−L shifted to lower wave numbers, which was possibly because of new Lewis acid sites (Ag−O) formation. While, after H_2 reduction the intensity of NH_4^+−B recovered and NH_3−L transferred back from Ag−O (1215 cm^{-1}) to Al−O (1252 cm^{-1}). Thus, we speculate that Ag species were anchored through the consumption of AlOH groups (Brønsted acid sites) and spread on the surface of Al_2O_3 with Ag−O bonds. The Ag^+ in Ag−O bonds acted as new Lewis acid sites to adsorb NH_3 and resulted in the red shift of IR absorption peaks. However, H_2 reduction breaks Ag−O bonds and thus recover the Brønsted acid sites. Meanwhile, metallic Ag agglomerated into small particle size, which led to the re-exposure of Al−O Lewis acid sites and also the blue shift of IR absorption peak of NH_3 peaks. The relationship between Ag loading and hydroxyl content confirmed the inference that Ag was anchored on the Al_2O_3 surface through Al−OH groups. The schematic diagram of the acid sites changes on Ag/Al_2O_3 catalyst before and after H_2 reduction is shown in Figure 10, side and top views of Ag/Al_2O_3 and $Ag/Al_2O_3-H_2$ were also provided, which can be used to show the change of Ag particle size after H_2 pretreatment.

The activity evaluation revealed that the NH_3−SCO activity on Ag/Al_2O_3 was notably improved after H_2 reduction. The T_{50} of NH_3−SCO decreased from 145 to 100 °C after the Ag/Al_2O_3 catalyst was pretreated with H_2. The NH_3 conversion rates on $Ag/Al_2O_3-H_2$ calculated based on kinetics testing were also significantly higher than those on Ag/Al_2O_3 (Figure S6, Supporting Information). The *in situ* DRIFTS revealed that the NH_3−SCO pathway followed the i-SCR mechanism on both Ag/Al_2O_3 and $Ag/Al_2O_3-H_2$ catalysts. When O_2 was introduced in, the NH_4^+−B on $Ag/Al_2O_3-H_2$ disappeared rapidly within 10 min, while NH_3−L maintained more than 20 min, the consumption rate of NH_4^+ ad-species was almost 5 times as fast as coordinated NH_3, indicating that the reactivity of NH_4^+ with O_2 was far higher than coordinated NH_3. In addition, when the reaction rates on Ag/Al_2O_3 and $Ag/Al_2O_3-H_2$ were normalized by the amount of acid sites (Figure S6, Supporting Information), the rate on per Brønsted site was higher than that on per Lewis site, further indicating that the Brønsted sites were favorable for the oxidation of NH_3.

Kinetic results showed that there were some differences in reaction pathways between two samples since E_a on $Ag/Al_2O_3-H_2$ (56.5 kJ/mol) was lower than that on Ag/Al_2O_3 sample (74.8 kJ/mol). DFT calculation results identified that the main differences in NH_3−SCO reaction pathways were due to the different activation processes for NH_4^+ and NH_3 species. The overall energy barrier for the activation of NH_4^+−B was 0.64 eV, much lower than that of NH_3−L (1.02 eV), further confirming that NH_4^+−B were more reactive than NH_3−L. Since the Brønsted acid sites have markedly higher activity than the Lewis acid sites, the fact that H_2 reduction recovered the Brønsted acid sites in $Ag/Al_2O_3-H_2$ should be an important reason for the improved NH_3−SCO activity of $Ag/Al_2O_3-H_2$. The possible NH_3−SCO reaction process over Ag/Al_2O_3 and $Ag/Al_2O_3-H_2$ is also diagramed in Figure 10.

DOI: 10.1021/acscatal.8b03744
ACS Catal. 2019, 9, 1437−1445

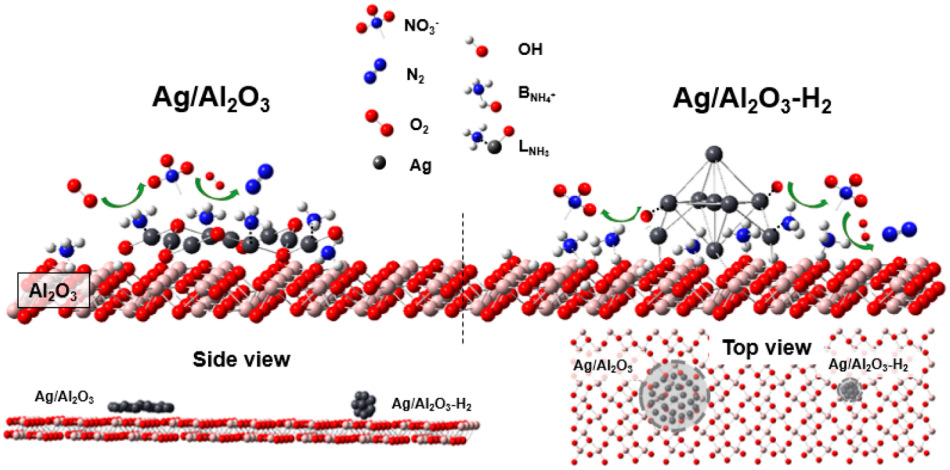

Figure 10. Diagram showing the possible NH_3−SCO reaction process over Ag/Al_2O_3 and Ag/Al_2O_3−H_2. Insets are side view and top view of Ag/Al_2O_3 and Ag/Al_2O_3−H_2.

5. CONCLUSIONS

In this paper, Ag/Al_2O_3 and H_2-pretreated Ag/Al_2O_3 catalysts were prepared and tested for NH_3−SCO. Characterization results revealed that Ag species was anchored on the Al_2O_3 surface through exchange between Ag^+ and H^+ in AlOH groups during the preparation process and then occupied the Brønsted acid sites of Al_2O_3. Ag loading made the Ag site function as the new Lewis acid site. H_2 reduction could break the Ag−O bonds, and this thus recovered the Brønsted acid sites. *In situ* DRIFTS revealed that the reaction pathway over Ag/Al_2O_3 and Ag/Al_2O_3−H_2 followed the i-SCR mechanism and that NH_4^+−B was much more active for reaction with O_2 than NH_3−L. The DFT calculation results confirmed that the activity of Brønsted acid sites is markedly higher than that for Lewis acid sites. Therefore, we conclude that the recovery of Brønsted acid sites due to H_2 reduction is also one of the important factors for the improvement of NH_3−SCO activity.

■ ASSOCIATED CONTENT

Supporting Information

The Supporting Information is available free of charge on the ACS Publications website at DOI: 10.1021/acscatal.8b03744.

^{27}Al MAS NMR spectra of Al_2O_3 and Ag/Al_2O_3, in situ DRIFTS of NH_3 adsorption and NH_3−SCO reaction at different temperatures, information on kinetic measurements, and normalization of reaction rates by Brønsted acid sites and Lewis acid sites (PDF)

■ AUTHOR INFORMATION

Corresponding Author

*(C.Z.) E-mail: cbzhang@rcees.ac.cn.

ORCID

Fei Wang: 0000-0002-4364-9956
Guangzhi He: 0000-0003-1770-3522
Changbin Zhang: 0000-0003-2124-0620

Notes

The authors declare no competing financial interest.

■ ACKNOWLEDGMENTS

This work was financially supported by the National Key R&D Program of China (2017YFC0211802, 2017YFC0211101) and the National Natural Science Foundation of China (21577159, 21777171).

■ REFERENCES

(1) Turšič, J.; Berner, A.; Podkrajšek, B.; Grgić, I. Influence of Ammonia on Sulfate Formation under Haze Conditions under Haze Conditions. *Atmos. Environ.* **2004**, *38*, 2789−2795.

(2) Pan, Y.; Tian, S.; Liu, D.; Fang, Y.; Zhu, X.; Zhang, Q.; Zheng, B.; Michalski, G.; Wang, Y. Fossil Fuel Combustion-Related Emissions Dominate Atmospheric Ammonia Sources During Severe Haze Episodes: Evidence from ^{15}n-Stable Isotope in Size-Resolved Aerosol Ammonium. *Environ. Sci. Technol.* **2016**, *50*, 8049−8056.

(3) Wang, G.; Zhang, R.; Gomez, M. E.; Yang, L.; Levy Zamora, M.; Hu, M.; Lin, Y.; Peng, J.; Guo, S.; Meng, J.; Li, J.; Cheng, C.; Hu, T.; Ren, Y.; Wang, Y.; Gao, J.; Cao, J.; An, Z.; Zhou, W.; Li, G.; Wang, J.; Tian, P.; Marrero-Ortiz, W.; Secrest, J.; Du, Z.; Zheng, J.; Shang, D.; Zeng, L.; Shao, M.; Wang, W.; Huang, Y.; Wang, Y.; Zhu, Y.; Li, Y.; Hu, J.; Pan, B.; Cai, L.; Cheng, Y.; Ji, Y.; Zhang, F.; Rosenfeld, D.; Liss, P. S.; Duce, R. A.; Kolb, C. E.; Molina, M. J. Persistent Sulfate Formation from London Fog to Chinese Haze. *Proc. Natl. Acad. Sci. U. S. A.* **2016**, *113*, 13630−13635.

(4) Chu, B.; Zhang, X.; Liu, Y.; He, H.; Sun, Y.; Jiang, J.; Li, J.; Hao, J. Synergetic Formation of Secondary Inorganic and Organic Aerosol: Effect of SO_2 and NH_3 on Particle Formation and Growth. *Atmos. Chem. Phys.* **2016**, *16*, 14219−14230.

(5) Chung, Y.; Huang, C.; Liu, C. H.; Bai, H. Biotreatment of Hydrogen Sulfide- and Ammonia-Containing Waste Gases by Fluidized Bed Bioreactor. *J. Air Waste Manage. Assoc.* **2001**, *51*, 163−172.

(6) Burch, R.; Southward, B. W. L. The Nature of the Active Metal Surface of Catalysts for the Clean Combustion of Biogas Containing Ammonia. *J. Catal.* **2001**, *198*, 286−295.

(7) Huang, T. L.; Cliffe, K. R.; Macinnes, J. M. The Removal of Ammonia from Water by a Hydrophobic Catalyst. *Environ. Sci. Technol.* **2000**, *34*, 4804−4809.

(8) Li, P.; Zhang, R.; Liu, N.; Royer, S. Efficiency of Cu and Pd Substitution in Fe-Based Perovskites to Promote N_2 Formation During NH_3 Selective Catalytic Oxidation (NH_3-SCO). *Appl. Catal., B* **2017**, *203*, 174−188.

(9) Gang, L.; Anderson, B. G.; van Grondelle, J.; van Santen, R. A. Intermediate Species and Reaction Pathways for the Oxidation of Ammonia on Powdered Catalysts. *J. Catal.* **2001**, *199*, 107−114.

(10) Gang, L.; Anderson, B. G.; van Grondelle, J.; van Santen, R. A.; van Gennip, W. J. H.; Niemantsverdriet, J. W.; Kooyman, P. J.; Knoester, A.; Brongersma, H. H. Alumina-Supported Cu−Ag Catalysts for Ammonia Oxidation to Nitrogen at Low Temperature. *J. Catal.* **2002**, *206*, 60−70.

DOI: 10.1021/acscatal.8b03744
ACS Catal. 2019, 9, 1437−1445

(11) Gang, L.; Anderson, B. G.; van Grondelle, J.; van Santen, R. A. Low Temperature Selective Oxidation of Ammonia to Nitrogen on Silver-Based Catalysts. *Appl. Catal., B* **2003**, *40*, 101−110.
(12) Yang, M.; Wu, C.; Zhang, C.; He, H. Selective Oxidation of Ammonia over Copper-Silver-Based Catalysts. *Catal. Today* **2004**, *90*, 263−267.
(13) Zhang, L.; He, H. Mechanism of Selective Catalytic Oxidation of Ammonia to Nitrogen over Ag/Al_2O_3. *J. Catal.* **2009**, *268*, 18−25.
(14) Zhang, L.; Zhang, C.; He, H. The Role of Silver Species on Ag/Al_2O_3 Catalysts for the Selective Catalytic Oxidation of Ammonia to Nitrogen. *J. Catal.* **2009**, *261*, 101−109.
(15) Qu, Z.; Wang, Z.; Quan, X.; Wang, H.; Shu, Y. Selective Catalytic Oxidation of Ammonia to N_2 over Wire−Mesh Honeycomb Catalyst in Simulated Synthetic Ammonia Stream. *Chem. Eng. J.* **2013**, *233*, 233−241.
(16) Jabłońska, M.; Nothdurft, K.; Nocuń, M.; Girman, V.; Palkovits, R. Redox-Performance Correlations in Ag−Cu−Mg−Al, Ce−Cu−Mg−Al, and Ga−Cu−Mg−Al Hydrotalcite Derived Mixed Metal Oxides. *Appl. Catal., B* **2017**, *207*, 385−396.
(17) Wang, F.; Ma, J.; He, G.; Chen, M.; Zhang, C.; He, H. Nanosize Effect of Al_2O_3 in Ag/Al_2O_3 Catalyst for the Selective Catalytic Oxidation of Ammonia. *ACS Catal.* **2018**, *8*, 2670−2682.
(18) Wang, F.; Ma, J.; He, G.; Chen, M.; Wang, S.; Zhang, C.; He, H. Synergistic Effect of TiO_2−SiO_2 in Ag/Si−Ti Catalyst for the Selective Catalytic Oxidation of Ammonia. *Ind. Eng. Chem. Res.* **2018**, *57*, 11903−11910.
(19) Newville, M. IFEFFIT: Interactive XAFS Analysis and FEFF Fitting. *J. Synchrotron Radiat.* **2001**, *8*, 322−324.
(20) Ravel, B.; Newville, M. Athena, Artemis, Hephaestus: Data Analysis for X-Ray Absorption Spectroscopy Using IFEFFIT. *J. Synchrotron Radiat.* **2005**, *12*, 537−541.
(21) Perdew, J. P.; Burke, K.; Ernzerhof, M. Generalized Gradient Approximation Made Simple. *Phys. Rev. Lett.* **1996**, *77*, 3865−3868.
(22) Grimme, S.; Antony, J.; Ehrlich, S.; Krieg, H. A Consistent and Accurate *ab Initio* Parametrization of Density Functional Dispersion Correction (DFT-D) for the 94 Elements H-Pu. *J. Chem. Phys.* **2010**, *132*, 154104−154123.
(23) Kresse, G.; Furthmuller, J. Efficient Iterative Schemes for *ab initio* Total-Energy Calculations Using a Plane-Wave Basis Set. *Phys. Rev. B: Condens. Matter Mater. Phys.* **1996**, *54*, 11169−11186.
(24) Kresse, G.; Joubert, D. From Ultrasoft Pseudopotentials to the Projector Augmented-Wave Method. *Phys. Rev. B: Condens. Matter Mater. Phys.* **1999**, *59*, 1758−1775.
(25) He, G.; Lian, Z.; Yu, Y.; Yang, Y.; Liu, K.; Shi, X.; Yan, Z.; Shan, W.; He, H. Polymeric Vanadyl Species Determine the Low-Temperature Activity of V-Based Catalysts for the Scr of NO_x with NH_3. *Sci. Adv.* **2018**, *4*, eaau4637−eaau4645.
(26) Henkelman, G.; Uberuaga, B. P.; Jonsson, H. A Climbing Image Nudged Elastic Band Method for Finding Saddle Points and Minimum Energy Paths. *J. Chem. Phys.* **2000**, *113*, 9901−9904.
(27) He, G.; Ma, J.; He, H. Role of Carbonaceous Aerosols in Catalyzing Sulfate Formation. *ACS Catal.* **2018**, *8*, 3825−3832.
(28) Chmielarz, L.; Jabłońska, M. Advances in Selective Catalytic Oxidation of Ammonia to Dinitrogen: A Review. *RSC Adv.* **2015**, *5*, 43408−43431.
(29) Hu, X.; Zhu, Q.; Wang, X.; Kawazoe, N.; Yang, Y. Nonmetal−Metal−Semiconductor-Promoted $P/Ag/Ag_2O/Ag_3PO_4/TiO_2$ Photocatalyst with Superior Photocatalytic Activity and Stability. *J. Mater. Chem. A* **2015**, *3*, 17858−17865.
(30) Pasricha, R.; Gupta, S.; Srivastava, A. K. A Facile and Novel Synthesis of Ag-Graphene-Based Nanocomposites. *Small* **2009**, *5*, 2253−2259.
(31) Zhang, Z.; Shao, C.; Sun, Y.; Mu, J.; Zhang, M.; Zhang, P.; Guo, Z.; Liang, P.; Wang, C.; Liu, Y. Tubular Nanocomposite Catalysts Based on Size-Controlled and Highly Dispersed Silver Nanoparticles Assembled on Electrospun Silicananotubes for Catalytic Reduction of 4-Nitrophenol. *J. Mater. Chem.* **2012**, *22*, 1387−1395.
(32) Nagai, Y.; Hirabayashi, T.; Dohmae, K.; Takagi, N.; Minami, T.; Shinjoh, H.; Matsumoto, S. Sintering Inhibition Mechanism of Platinum Supported on Ceria-Based Oxide and Pt-Oxide−Support Interaction. *J. Catal.* **2006**, *242*, 103−109.
(33) Sandoval, A.; Aguilar, A.; Louis, C.; Traverse, A.; Zanella, R. Bimetallic Au−Ag/TiO_2 Catalyst Prepared by Deposition−Precipitation: High Activity and Stability in CO Oxidation. *J. Catal.* **2011**, *281*, 40−49.
(34) Verma, P.; Yuan, K.; Kuwahara, Y.; Mori, K.; Yamashita, H. Enhancement of Plasmonic Activity by Pt/Ag Bimetallic Nanocatalyst Supported on Mesoporous Silica in the Hydrogen Production from Hydrogen Storage Material. *Appl. Catal., B* **2018**, *223*, 10−15.
(35) Zhou, W.; Li, T.; Wang, J.; Qu, Y.; Pan, K.; Xie, Y.; Tian, G.; Wang, L.; Ren, Z.; Jiang, B.; Fu, H. Composites of Small Ag Clusters Confined in the Channels of Well-Ordered Mesoporous Anatase TiO_2 and Their Excellent Solar-Light-Driven Photocatalytic Performance. *Nano Res.* **2014**, *7*, 731−742.
(36) Topsoe, N.-Y. Mechanism of the Selective Catalytic Reduction of Nitric Oxide by Ammonia Elucidated by in Situ on-Line Fourier Transform Infrared Spectroscopy. *Science* **1994**, *265*, 1217−1219.
(37) Amores, J. M. G.; Escribano, V. S.; Ramis, G.; Busca, G. An Ft-Ir Study of Ammonia Adsorption and Oxidation over Anatase-Supported Metal Oxides. *Appl. Catal., B* **1997**, *13*, 45−58.
(38) Ramis, G.; Yi, L.; Busca, G.; Turco, M.; Kotur, E.; Willey, R. J. Adsorption, Activation, and Oxidation of Ammonia over SCR Catalysts. *J. Catal.* **1995**, *157*, 523−535.
(39) Liu, F.; He, H.; Ding, Y.; Zhang, C. Effect of Manganese Substitution on the Structure and Activity of Iron Titanate Catalyst for the Selective Catalytic Reduction of NO with NH_3. *Appl. Catal., B* **2009**, *93*, 194−204.
(40) Lian, Z.; Liu, F.; He, H.; Shi, X.; Mo, J.; Wu, Z. Manganese−Niobium Mixed Oxide Catalyst for the Selective Catalytic Reduction of NOx with NH_3 at Low Temperatures. *Chem. Eng. J.* **2014**, *250*, 390−398.
(41) Ramis, G.; Yi, L.; Busca, G. Ammonia Activation over Catalysts for the Selective Catalytic Reduction of NOx and the Selective Catalytic Oxidation of NH_3. An FT-IR Study. *Catal. Today* **1996**, *28*, 373−380.
(42) Long, R. Q.; Yang, R. T. Selective Catalytic Reduction of Nitrogen Oxides by Ammonia over Fe^{3+}-Exchanged TiO_2-Pillared Clay Catalysts. *J. Catal.* **1999**, *186*, 254−268.
(43) Kwak, J. H.; Hu, J.; Mei, D.; Yi, C.-W.; Kim, D. H.; Peden, C. H. F.; Allard, L. F.; Szanyi, J. Coordinatively Unsaturated Al^{3+} Centers as Binding Sites for Active Catalyst Phases of Platinum on γ-Al_2O_3. *Science* **2009**, *325*, 1670−1673.
(44) Ballinger, T. H.; Yates, J. T., Jr Ir Spectroscopic Detection of Lewis Acid Sites on $A1_2O_3$ Using Adsorbed CO. Correlation with Al-OH Group Removal. *Langmuir* **1991**, *7*, 3041−3045.
(45) Jacobsen, C. J. H.; Topsøe, N. Y.; Topsøe, H.; Kellberg, L.; Jakobsen, H. J. Quantitative ^1H MAS NMR Studies of Structurally Different OH Surface Groups on η-Al_2O_3 and Mo/η-Al_2O_3 Catalysts. *J. Catal.* **1995**, *154*, 65−68.
(46) Lin, S. D.; Gluhoi, A. C.; Nieuwenhuys, B. E. Ammonia Oxidation over Au/MOx/γ-Al_2O_3—Activity, Selectivity and FTIR Measurements. *Catal. Today* **2004**, *90*, 3−14.
(47) Wu, J.; Cheng, Y. In Situ Ftir Study of Photocatalytic No Reaction on Photocatalysts under UV Irradiation. *J. Catal.* **2006**, *237*, 393−404.
(48) Pozdnyakov, D. V.; Filimonov, V. N. Infrared Study of Molecular Complexes Arising from Adsorption of NO and NO_2 on the Surface of Oxides. *Adv. Mol. Relax. Processes* **1973**, *5*, 55−63.
(49) Hadjiivanov, K.; Bushev, V.; Kantcheva, M.; Klissurski, D. Infrared Spectroscopy Study of the Species Arising During NO_2 Adsorption on TiO_2 (Anatase). *Langmuir* **1994**, *10*, 464−471.
(50) Zhang, R.; Yang, W.; Luo, N.; Li, P.; Lei, Z.; Chen, B. Low-Temperature NH_3-SCR of NO by Lanthanum Manganite Perovskites: Effect of A-/B-Site Substitution and TiO_2/CeO_2 Support. *Appl. Catal., B* **2014**, *146*, 94−104.

DOI: 10.1021/acscatal.8b03744
ACS Catal. 2019, 9, 1437−1445